WARSAW UNIVERSITY OF TECHNOLOGY Index 351733
FACULTY OF CIVIL ENGINEERING
COMMITTEE FOR CIVIL AND WATER ENGINEERING
POLISH ACADEMY OF SCIENCES ISSN 1230-2945

DOI: 10.24425/ace.2025.154123
ARCHIVES OF CIVIL ENGINEERING
Vol. LXXI ISSUE 2 2025
pp. 313–330

Research paper

Wind load equivalence method and structural response analysis of large-span space steel structures

Yonggang Chen[1], Jianming Ceng[2], Zhiming Yu[3], Yukai Wang[4], Li Gong[5], Tengteng Yang[6]

Abstract: In coastal areas, large-span space steel net trusses experience structural deformation due to strong winds. Currently, the application of equivalent static wind load to the structure does not consider the influence of local forces. The local uneven force on the bars caused by the structural appearance is ignored, complicating the identification of local deformation in the net truss. Additionally, this simplification increases the difficulty in evaluating wind load-sensitive areas of the building. This paper introduces a novel method for calculating static equivalent wind load, considering the transmission relationship between the structural roofs appearance and the internal truss forces. Following the outlined methodology, wind load is precisely applied at nodes with diverse windward faces, taking into account the node area ratio. The paper also examines how varying standard wind load values affect mesh truss deformation under different wind angles. Results indicate that, at 0°, 90°, 180°, and 270° wind directions, wind load-sensitive areas are linked to roof shape and structural characteristics. Maximum displacement in the truss grid's overall structure primarily occurs in the windward corner contact area. Network truss deformation linearly increases with the load standard. If the wind load exceeds 1.0 kN/m^2, deformation is associated with the windward vertical plane's area and steel column spacing, impacting overall structural safety.

Keywords: large-span spatial structure, numerical simulation, statical analysis, equivalent static wind load

[1]Eng., Railway Division, China Railway Construction Engineering Fifth Construction Co., Guangzhou 510000, China, e-mail: 6485004510@qq.com, ORCID: 0009-0005-7931-3177
[2]Eng., Engineering Quality Supervision Station, China Railway Guangzhou Group Co.,Ltd. Guangzhou510000, China, e-mail: hewu5901@126.com, ORCID: 0009-0000-3570-8461
[3]Eng., Station Building Construction Headquarters, China Railway Guangzhou Group., Ltd, Guangzhou510000, China, e-mail: 22834066@qq.com, ORCID: 0009-0009-8343-8334
[4]Eng., Railway Division, Station building construction headquarters, China RailwayConstruction Engineering Fifth Construction Co., Guangzhou510000, China, e-mail: 283868793@qq.com, ORCID: 0009-0004-0581-7391
[5]Prof., PhD., School of Civil Engineering, Lanzhou Jiaotong University, Lanzhou730070, China, e-mail: gongl@mail.lzjtu.cn, ORCID: 0000-0002-4824-5109
[6]MSc., School of Civil Engineering, Lanzhou Jiaotong University, Lanzhou730070, China, e-mail: 2680673647@qq.com, ORCID: 0000-0002-2711-5014

1. Introduction

Large-span spatial steel roofs are typical wind-sensitive structures. However, due to their inherent structural characteristics, such as light mass, flexibility, and a low natural vibration frequency [1–3], they are extensively utilized in prominent public buildings, including railroad passenger stations. Nevertheless, the structural design encounters numerous engineering challenges, particularly when subjected to strong winds [4, 5]. In the typhoon-prone regions along the coast of China, structural damage induced by wind leads to localized harm or destruction of large-span spatial steel structures, culminating in significant economic losses to both lives and property [6, 7].

In practical construction, the distinctive and innovative appearance of the net truss structure design prompts the utilization of the Equivalent Static Wind Load (ESWL) method to calculate the impact of strong winds on the roof structure [8]. This method, employed to assess the structure's response to wind load, aims to simplify the intricate randomized wind forces into a static force load [9]. However, limitations arise in conducting structural static analysis, including insufficient consideration of the transmission relationship between the structural roof's exterior shape and the internal web truss forces. Furthermore, there is a lack of attention to the issue of local force heterogeneity in the bars, induced by the structure's exterior characteristics. This heterogeneity leads to wind load influencing the local nodes of the web trusses, with no significant variance in the static force of the local area [10]. During the steel structure design process and the evaluation of the overall load carrying capacity, the bars uniformly experience wind load. However, the prediction of node displacement fails to accurately pinpoint the sensitive area of structural wind load. Consequently, achieving structural optimization design based on structural deformation becomes challenging [11]. In light of this, a more precise analysis of the uneven force at the local nodes, attributed to the net truss structure's shape, is essential for the accurate assessment of its deformation.

Currently, scholars both at home and abroad have undertaken extensive research on the impact of wind on the deformation of steel buildings [12]. Finite element simulation is commonly employed to predict the structure's deformation. Ma et al. [13]. used ANSYS to establish the finite element modeling of the roof structure and analyzed the wind performance and equivalent static wind load of a large-span openable truss structure. Li et al. [14] investigated the wind response of the large-span airsupported membrane structure coal scaffolding under the influence of typhoons and obtained the displacement response by finite element software ANSYS to calculate the displacement response. Xu et al. [15] took Dongsheng Station of the Guangzhou-Zhuhai Intercity Rail Transit Project as an example and conducted a relevant study on the wind load of the roof structure when the train passes the station. WO et al. [16] analyzed the roof structure deformation of the Zhanjiang New Airport terminal building using zonal multiobjective equivalent static wind load. However, there are fewer studies on the conversion of wind load acting on surface forces and nodal static loads for large-span roofs in strong typhoon regions, especially on the stress performance of large-span steel roof mesh truss structures under different standard values of wind loads [17, 18].

In summary, this paper proposes a steel structure wind load equivalence method based on the force transfer relationship between the outer wall surface of the roof cover and the mesh

truss, and calculates the static wind load at the contact node between the roof cover and the rods. Taking Xintang Station in Guangzhou, China, as an example, ANSYS finite element software is used to analyze the deformation response characteristics of steel mesh trusses, and to explore the displacement response of the large-span steel mesh truss structure under different wind loads at various wind angles at the forming structure.

2. A static equivalent method of wind load

In order to apply static wind loads reasonably to the nodes of large-span space steel structures, this paper proposes a new computational method for the static equivalent application of wind load, and the flow of the equivalent method is shown in Fig. 1. This method is mainly applied to the equivalent application of node loads on the facial region. Firstly, at the structural acting face level, it is necessary to assess the appearance shape of the structure and calculate the length and width of the force surface to obtain the area of the vertical windward face [19]. Second, at the net truss node level, the location of the bars, the number of nodes, and the direction of the force need to be determined. Then, using the method of target node area cutting, the wind load in the facial area is assigned to the structural rod nodes according to the area ratio, so as to obtain the static load of a single node as shown in Eq. (2.1):

$$F_i = w_k hb \frac{S_i}{S_{\text{total}}} \tag{2.1}$$

where: F_i – the node static load, kN, w_k – the standard value of wind load, kN/m^2; h – the length of the vertical windward surface, m; b – the width of the vertical windward surface, m; S_{total} – the total area of the structure, m^2; S_i – the node of the area occupied, m^2.

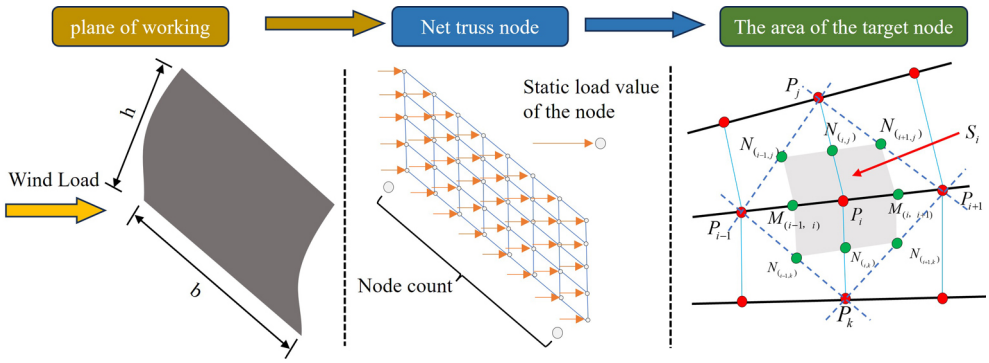

Fig. 1. Static Equivalent Method of Wind Load

In order to calculate the area occupied by the i node, assuming any target node $P_i = (x_i, y_i, z_i)$,with adjacent bars having four nodes P_{i-1}, P_{i-2}, P_{i-2} and P_{i+2}, calculate the midpoint coordinates of the target node, and their midpoints $M_{(i,i-1)}$, $N_{(i-1,j)}$ and $N_{(i-1,k)}$, as shown in Eq. (2.2), Eq. (2.3), and Eq. (2.4).

$$M_{(i,i-1)} = \left(\frac{x_i + x_{i-1}}{2}, \frac{y_i + y_{i-1}}{2}, \frac{z_i + z_{i-1}}{2} \right) \tag{2.2}$$

$$N_{(i-1,j)} = \left(\frac{x_{i-1} + x_j}{2}, \frac{y_{i-1} + y_j}{2}, \frac{z_{i-1} + z_j}{2} \right) \tag{2.3}$$

$$N_{(i-1,k)} = \left(\frac{x_{i-1} + x_k}{2}, \frac{y_{i-1} + y_k}{2}, \frac{z_{i-1} + z_k}{2} \right) \tag{2.4}$$

The formula for calculating the area of the quadrilateral formed by the target node P_i and its adjacent midpoints $M_{(i,i-1)}$, $N_{(i-1,j)}$ and $N_{(i-1,k)}$. Assuming the target node is the i node, the area of the quadrilateral occupied by the target node i is given by Eq. (2.5).

$$S_i = \frac{1}{2} \left[\begin{array}{l} \left\| (\overline{P_i N_{(i-1,j)}} \times \overline{M_{(i-1,i)} N_{(i,j)}} \right\| + \left\| (\overline{P_i N_{(i+1,j)}} \times \overline{M_{(i,i+1)} N_{(i,j)}} \right\| \\ + \left\| (\overline{P_i N_{(i-1,k)}} \times \overline{M_{(i-1,i)} N_{(i,k)}} \right\| + \left\| (\overline{P_i N_{(i+1,k)}} \times \overline{M_{(i,i+1)} N_{(i,k)}} \right\| \end{array} \right] \tag{2.5}$$

At the same time, the total area of the structural outer surface can be obtained, calculated as shown in Eq. (2.6):

$$S_{\text{total}} = \sum_{i=1}^{N} s_I \tag{2.6}$$

Based on the above calculation method, the nodal area of each bar in the model is calculated using MATLAB software programming to obtain accurate nodal static loads.

3. Model and load value extraction

3.1. Engineering background

This paper takes the net truss of Xintang Station in Xintang Town, Zengcheng District, Guangzhou City, as an example, to analyze the static characteristics of the net truss. The roof structure adopts the net truss combination system, with a quadrangular conical net frame structure on the north and south sides, triangular trusses in the middle part, and the nodes adopt the welded ball node, which is a typical large-span steel structure roof. The schematic diagram of the net truss structure is shown in Fig. 2.

3.2. Model parameter sensitivity analysis

In finite element modeling of steel mesh trusses, element type and element count are key sensitive parameters in the model calculation. In this study, the upper web members are depicted schematically in Fig. 3(a). They are 4500 mm in length with a section size of D299 × 14 mm, and the concentrated force at the end is P = 20 kN. Beam188 and Beam189 elements are used for modeling. The effects of element type and number of elements on the structural deformation are compared and analyzed.

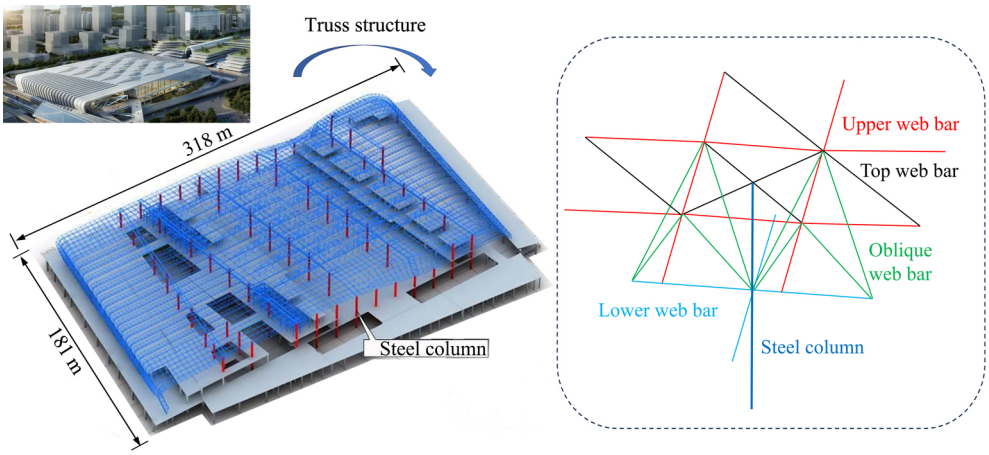

Fig. 2. Schematic diagram of the structure of the network truss

Figure 3(b) shows the displacement variation maps for different element types and mesh sizes. The element types used are Beam188 and Beam189, and the mesh sizes are set to 2, 20, and 100 divisions for three working conditions. From Fig. 3, it is observed that the displacement and rod deformation maps calculated using Beam188 and Beam189 elements are identical. Additionally, the number of mesh divisions has no effect on the structural deformation of the beam elements. are identical. Additionally, the number of mesh divisions has no effect on the structural deformation of the beam elements.

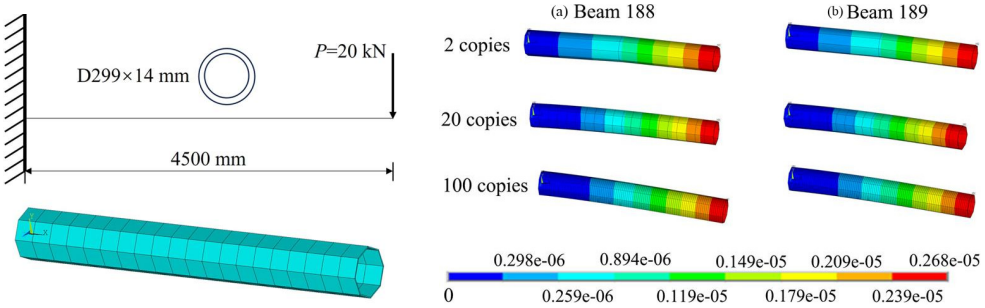

(a) Schematic diagram of web rods (b) Element type and mesh size

Fig. 3. Model parameter sensitivity analysis;
(a) Schematic diagram of web rods, (b) Element type and mesh size

3.3. Model building

ANSYS and CAD modeling were combined to create the roof net truss finite element model [20]. The finite element model was established by selecting roof transverse trusses, vertical trusses (including truss chords, and web rods), steel columns, and roof net frames. We defined different crosssection sizes to distinguish the steel pipe diameter, then simulated

and calculated the pipe diameter of the steel column as D1300 × 40 mm. We simplified the rest of the truss rods and net frame crosssections to the same crosssection and chose the smallest crosssection size, D299 × 14 mm. In the static analysis, the stresses of the structural rods may be more than the yield stresses of the steel, and the elasticplastic properties of the rod materials should be considered. The elasticplastic properties were analyzed using the geometric nonlinearity of ANSYS, and the unit type was set as Beam188 unit, which considers the elasticplastic properties of the material as well as the effects of large displacements, large rotations, and shear deformations of the rods [21]. The rods were connected through the common node, and the restraining boundary conditions were applied at the bottom end of the steel column and the contact nodes of the two sides of the bending landing and the concrete structure of the waiting floor. The degrees of freedom in each direction were restrained, i.e., six directions, UX, UY, UZ, ROTX, ROTY, and ROTZ [22]. The finite element model of the three dimensional curved roof main web truss mesh frame is shown in Fig. 4.

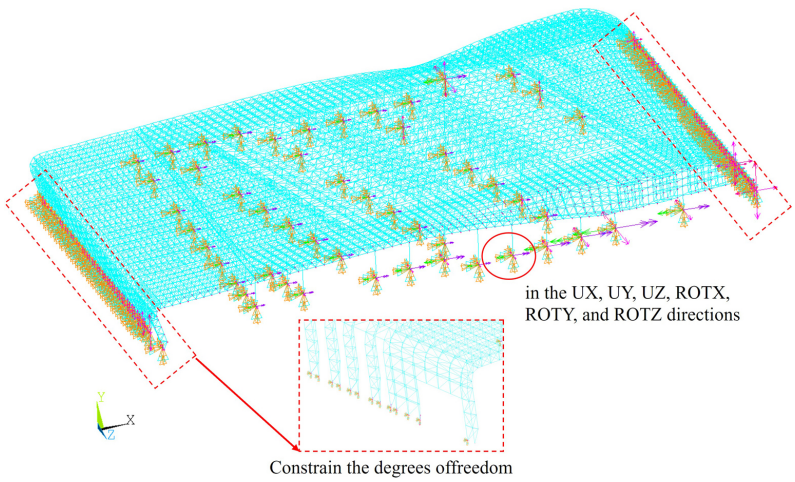

Fig. 4. The finite element model of the three-dimensional

3.4. Steel material parameter acquisition

In order to obtain the intrinsic stress-strain relationship of Q355B material, a set of quasistatic tensile tests were carried out with the test environment temperature of 20° [23]. The specimens used in the experiment were cut and processed from Q355B steel pipe with a thickness of H = 0.05 m, and the specimen test equipment and the fractured specimen after tensile are shown in Fig. 5. In the ANSYS static analysis, the net truss structure material is defined as a multilinear material model, and the stress-strain curve is shown in Fig. 6, with a tensile strength of 489 MPa, a yield strength of 317 MPa, and a total elongation of 10.5% at the maximum force.

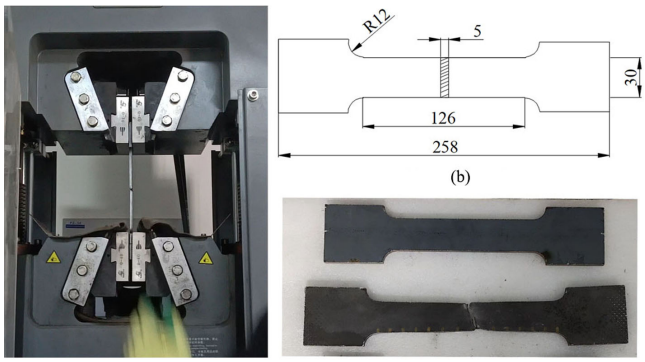

Fig. 5. Specimen equipment and post-tension fracture specimens; (a) Universal material testing machine, (b) Specimen size, (c) Fracture specimen after tensile test

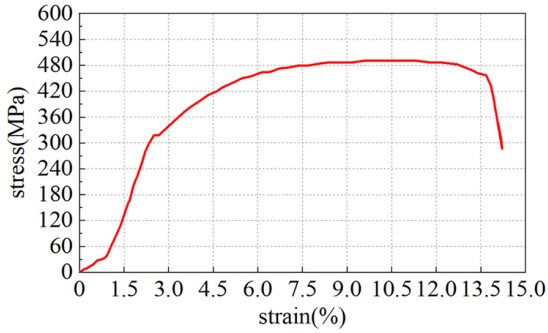

Fig. 6. Q355B stress-strain curve

3.5. Values of angular wind loads for different wind directions

The project is located in Zengcheng District, Guangzhou City, Guangdong Province, according to the relevant provisions of the Code for Structural Loading of Buildings (GB 50009-2012) [24]. The basic wind pressure in this study was 0.6 kN/m^2, the terrain was flat, the height of the building was 35.65 m, and the degree of roughness of the ground was class B. The coefficient of variation of the height of the wind pressure was determined to be 1.39, and the value of the wind vibration coefficient according to the value of 100-year one time occurrence was 1.6. The body coefficient is shown in Fig. 7, which calculates the main stress structure. The standard value of wind load perpendicular to the building's surface can be expressed as Eq. (3.1):

$$W_k = \beta_z \mu_s \mu_z W_0 \tag{3.1}$$

where: W_k – the standard value of wind load (kN/m^2), β_z – the wind vibration coefficient at height z, μ_s – the wind load body type coefficient, μ_z – the wind pressure height change coefficient, W_0 – the basic wind pressure (kN/m^2).

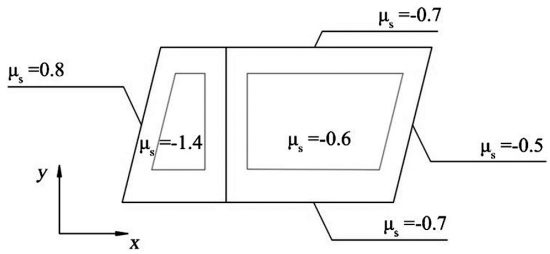

Fig. 7. Roof shape coefficient distribution

4. Static Analysis of the Main Truss Structure of Roof

Wind load is a type of surface load whose direction is perpendicular to the windward surface, and different wind directions have a great influence on the internal mesh truss structure. In this paper, according to the characteristics of the structure, static analysis is carried out at four direction angles of 0°, 90°, 180°, and 270° [25]. The positions of different wind direction angles are shown in Fig. 8. Using the static equivalent method of wind load proposed in this paper, six standard load values are applied to the surface of the outer cover. The displacement components in the x, y, and z directions, as well as the total displacement, are then analyzed under different load conditions.

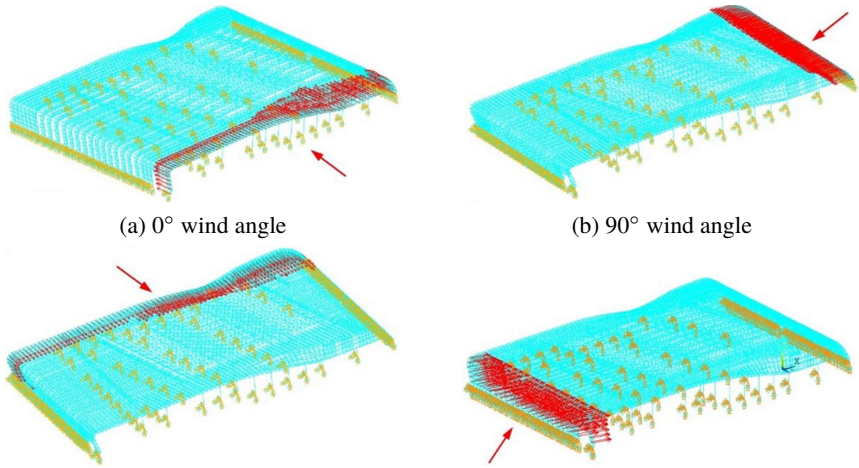

(a) 0° wind angle (b) 90° wind angle

(c) 180° wind angle (d) 270° wind angle

Fig. 8. The 0° (a), 90° (b), 180° (c), and 270° (d) wind direction angle diagram

4.1. Relationship between wind loads and structurally sensitive areas

The characteristics of large-span space steel structure roofs and wind load values are crucial for structural design [26]. Figure 9 shows the displacement cloud diagram for different wind loads. Observing the displacement cloud diagram under four different wind load standard values

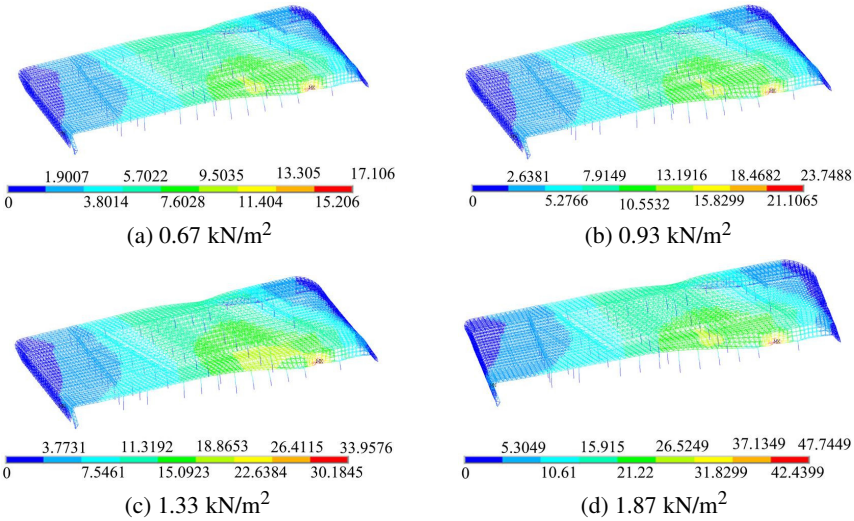

(a) 0.67 kN/m^2 (b) 0.93 kN/m^2

(c) 1.33 kN/m^2 (d) 1.87 kN/m^2

Fig. 9. Displacement map under different standard values of wind loads; (a) 0.67 kN/m^2, (b) 0.93 kN/m^2, (c) 1.33 kN/m^2, (d) 1.87 kN/m^2

reveals that the structural deformation of roof mesh trusses occurs at the same location. The larger the wind load, the more pronounced the structural deformation. This deformation is not affected by the wind load acting on the roof surface, indicating that the sensitive area of the steel roof net truss is related to the roof shape and structural characteristics.

The above analysis shows that the wind load standard value had less influence on the wind load sensitive area of the net truss. The maximum displacement was in the same position under the action of different wind load standard values, and the structural deformation of the net truss was analyzed only for the typical load standard value of 0.67 kN/m^2.

4.2. Deformation of main net truss structure at 0° wind angle

Figure 10 shows the displacement cloud diagram of the main roof truss under typical working conditions with a standard wind load of 0.67 kN/m^2. When the vertical wind blew the main roof truss, there was a significant difference in the displacement in different directions and the total displacement change. From Fig. 10(a), we see that the maximum displacement in the x-direction occurred in the corner area of the windward side, i.e., in the contact area between wind load and web trusses; the web trusses are tensile under the wind load and cause deformation of the neighboring side of the structure. Fig. 10(b) shows the maximum displacement in the y-direction was mainly concentrated on the opposite side of the wind load and the roof surface, and the deformation of the roof surface was caused by the joint action of gravity and wind suction. From Fig. 10(c), we know that the deformation of the two sides of the net truss in the z-direction was the smallest, which is mainly due to the wind load direction being the same as the deformation direction; the deformation of the structure was mainly in the contacting area of the corners of the windward side. From Fig. 10(d), the maximum displacement of the overall net truss structure was mainly concentrated in the corner

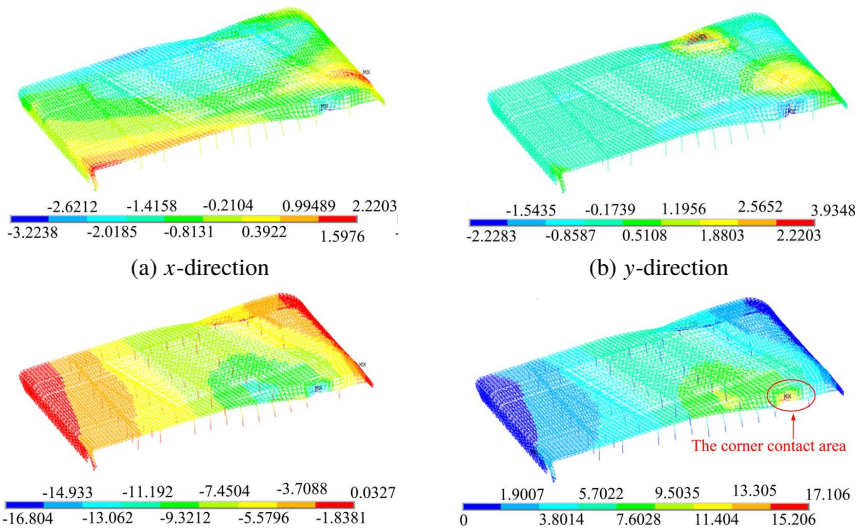

(a) x-direction (b) y-direction

(c) z-direction (d) Total displacement deformation

Fig. 10. The 0° wind direction angle (0.67 kN/m^2) truss grid deformation; (a) x-direction, (b) y-direction, (c) z-direction, (d) Total displacement deformation

contact area of the net truss surface where the maximum wind load contacts. The deformation expanded from the maximum contact surface of the wind load in the form of a bow wave to the surroundings in order, and with increased distance, the overall displacement and deformation of the overall structure of the net truss decreased.

Figure 11 shows the maximum displacement value of the net truss under different load standard values at a 0° wind angle. With increased wind load, the displacement in the x-, y-, and z-directions and the total displacement of the net trusses increased. The wind load

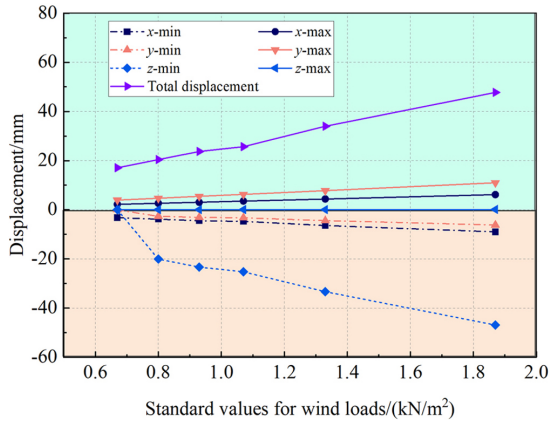

Fig. 11. Maximum displacement of the structure for different standard values of wind loads (The 0° wind direction angle)

had a linear relationship with structural change. The wind load sensitive zone of the roof main web truss structure appeared in the windward side area; the leeward side had less influence, and the wind load size had less influence on the wind load sensitive zone of the roof web truss.

4.3. Deformation of main net truss structure at 90° wind angle

Figure 12 shows the displacement cloud diagram of the main roof truss under typical working conditions with a standard wind load of 0.67 kN/m^2. From Fig. 12(a), the maximum displacement in x-direction appears in the center roof of the contact area of the wind load, and the deformation is minimum at the steel columns and the connection with the concrete. The maximum displacement in the x-direction occurs in the center roof of the wind–loaded contact area, the steel columns and mesh trusses had the least deformation at the concrete connections, and the deformation in the x-direction was consistent with the overall structure deformation. From Fig. 12(b), the maximum deformation in the y-direction was mainly concentrated in the wind load contact area and the roof surface, and the deformation of the net frame on the roof surface was mainly distributed between the main trusses. From Fig. 12(c), the minimum deformation in the z-direction of the roof web trusses indicates that the lateral stiffness of the structure is strong. From Fig. 12(d), the maximum displacement of the overall structure of the net truss was mainly concentrated in the net truss surface with the largest wind load contact; the deformation extended from the surface of the largest wind load contact in the form of a bow wave to the surroundings. With increased distance, displacement was uniformly transmitted along the negative x-direction, and the deformation decreased, so the net truss deformation was uniformly and symmetrically distributed.

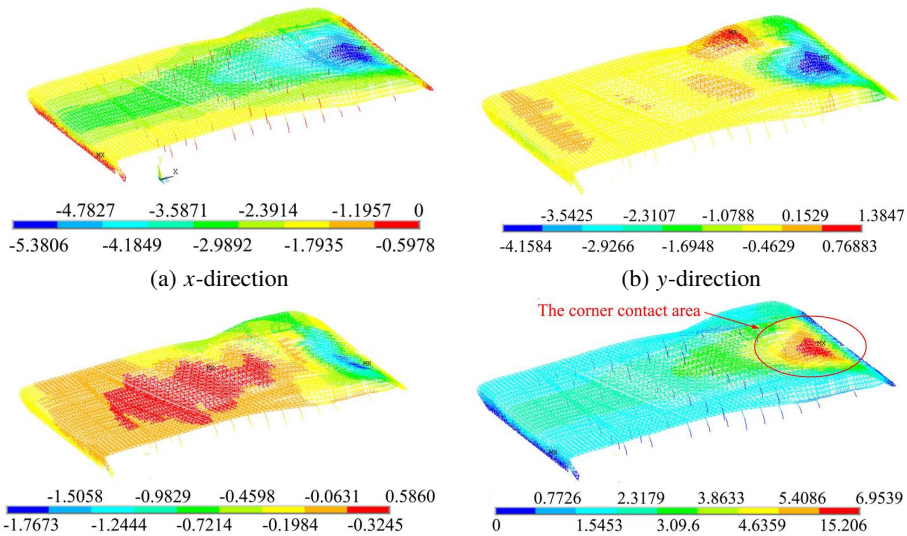

Fig. 12. The 90° wind direction angle (0.67 kN/m^2) truss grid deformation; (a) x-direction, (b) y-direction, (c) z-direction, (d) Total displacement deformation

Figure 13 shows the maximum displacement value of the net truss under different load standard values at 90°. With the increased wind load standard value, the displacement generated by the structural net truss also increased, and its wind load standard value had a linear relationship with the deformation displacement of the structure, and the size of the total displacement was consistent with that of the x-direction displacement. The results show that the deformation of the net truss roof under a 90° wind load is in the edge corner area of the contact angle imposed by wind load.

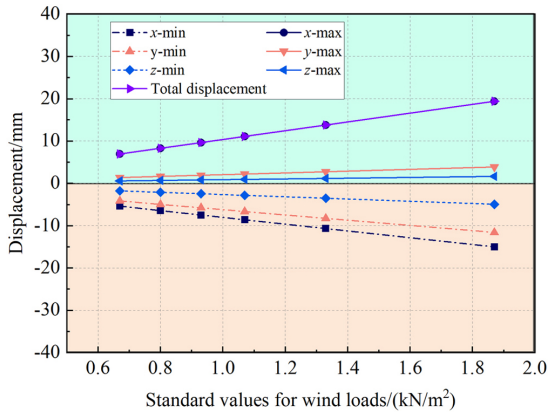

Fig. 13. Maximum displacement of the structure for different standard values of wind loads (The 90° wind direction angle)

4.4. Deformation of main net truss structure at 180° wind angle

Figure 14 shows the displacement cloud diagrams of the main web truss for the roof cover with a typical wind load standard value of 0.67 kN/m^2 at a 180° wind angle. Fig. 14(a) shows that the maximum displacement in the x-direction occurs in the contact corner area of the windward face. The left and right surfaces of the roof were not uniformly loaded, and the displacement of the left side of the windward face was larger than that of the right side, which is related to the loaded area of the web trusses. Fig. 14(b) shows that the maximum displacement in the y-direction was mainly concentrated in the contact area of wind load on the left windward side and the backward side, and it is worth noting that the deformation of the net truss on the right side of the wind loaded contact area was smaller. Fig. 14(c) and Fig. 14(d) show the deformation of the net truss in the z-direction and the total deformation of the whole structure. The maximum displacement was mainly concentrated in the corner area of the net truss with maximum contact with the wind load; at the same time, the roof cover deformation was extended from the maximum contact surface of the wind load in the form of a bow wave in the four directions, and with the increased distance, the displacement and deformation decreased, and the deformation of the truss net truss presented as symmetrically distributed with a relatively uniform force.

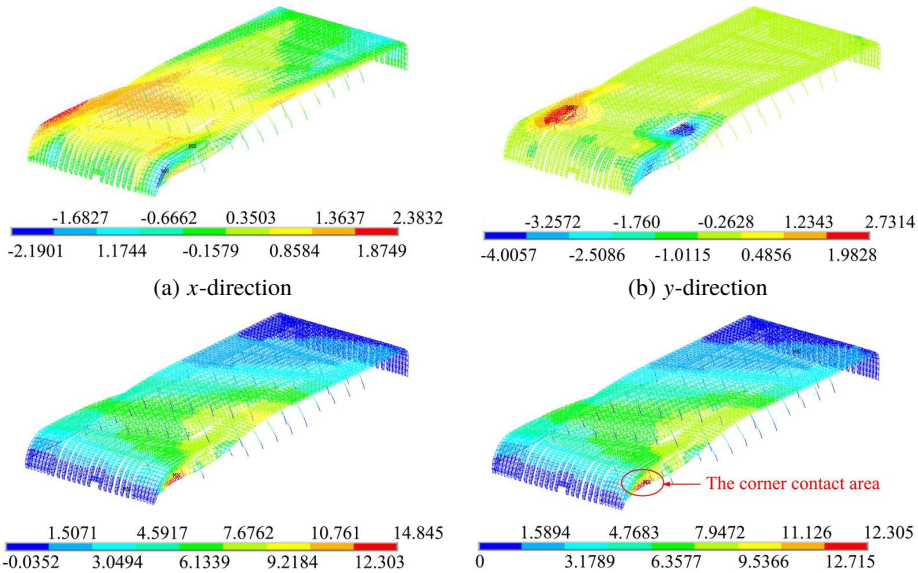

Fig. 14. The 180° wind direction angle (0.67 kN/m^2) truss grid deformation; (a) x-direction, (b) y-direction, (c) z-direction, (d) Total displacement deformation

Figure 15 shows the maximum displacement value of the truss net frame under different load standard values at a 180° direction angle. The displacement of the net truss increased with the standard value of the wind load. There was a linear relationship between different load standard values and the maximum displacement value of the truss net frame at 180°.

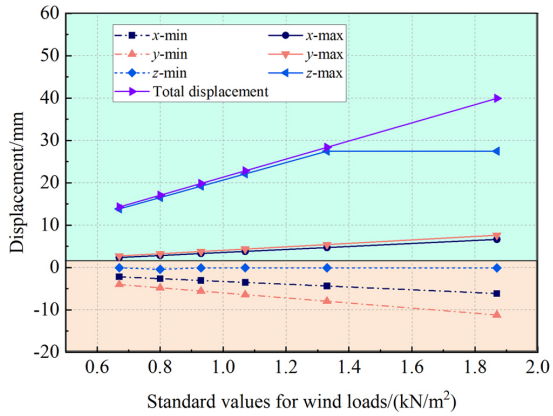

Fig. 15. Maximum displacement of the structure for different standard values of wind loads (The 180° wind direction angle)

4.5. Deformation of main net truss structure at 270° wind angle

Figure 16 shows the structural deformation of the main trusses of the roof with the typical wind load standard value of 0.67 kN/m^2 at a 270° wind angle. Fig. 16(a) shows that the maximum displacement of the truss in the x-direction is mainly concentrated at the corners of the connection between the supporting frame and the roof frame. The deformation of the truss on the roof surface extended in the form of a bow wave from the maximum contact surface of the wind load to the surroundings, and with the increased distance, the displacement and deformation decreased, and the deformation was symmetrically distributed in both the left and right directions. From Fig. 16(b), the maximum displacement in the y-direction was mainly concentrated on the opposite side of the wind load contact area. This is because the spacing of the steel columns at this location is large, which leads to the deformation of the roof trusses. From Fig. 16(c), the maximum displacement of the net truss appeared in the center of the supporting net frame and roof cover, and the deformation of the structure on the side far away from the wind load was small and almost not affected by the wind load. From Fig. 16(d), the maximum displacement of the steel roof net joist was mainly concentrated in the connection of the supporting net frame and roof net frame. The deformation of the roof net joist was extended from the maximum contact surface of wind load to all directions in the form of a bow wave; the deformation of the net joist was symmetrically distributed in both the left and right directions. The biggest difference with the net joist deformation in the x-direction was a big displacement in a small portion of the roof net joist in the side away from wind load. The reason for this deformation was a supporting net frame in the area, which was almost unaffected by wind

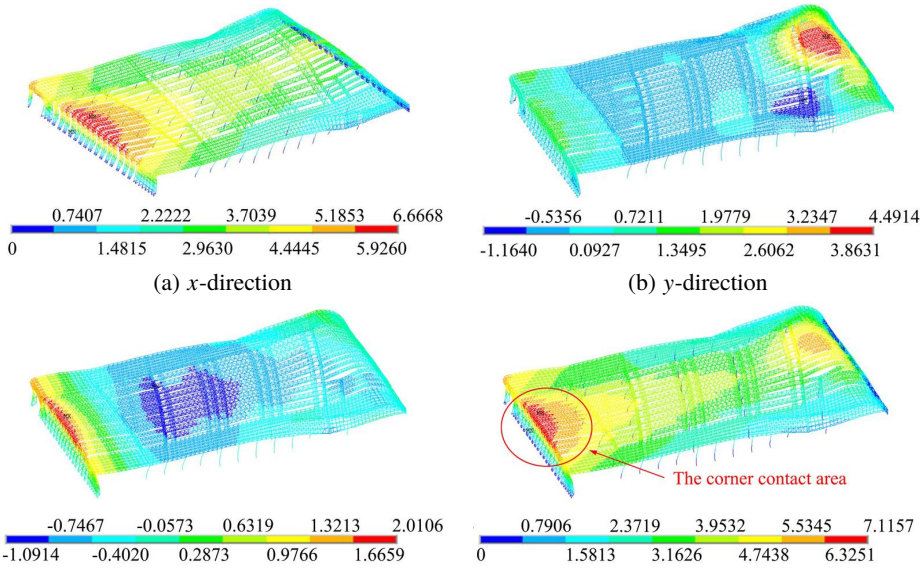

Fig. 16. The 270° wind direction angle (0.67 kN/m^2) truss grid deformation; (a) x-direction, (b) y-direction, (c) z-direction, (d) Total displacement deformation

load. The biggest difference in the x-direction deformation of the net truss was that a small part of the roof cover on the side away from the wind load had a big displacement [27].

The maximum displacement of the truss net frame under different load standard values at 270° direction angle is given in Fig. 17, from which it can be found that the displacement of the truss net frame increases with the increase of the standard value of wind load, and there is a linear correlation between the two.

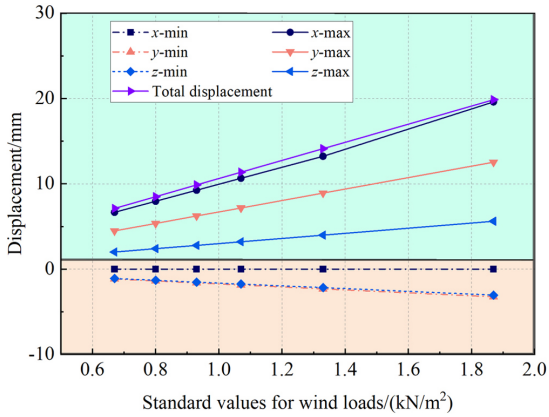

Fig. 17. Maximum displacement of the structure for different standard values of wind loads (The 270° wind direction angle)

5. Analysis of overall deformation of mesh truss under the combination of wind angle and standard value of wind load

Through the above analysis of the single factor influence on the net truss with different wind angles and wind loads, we see that the maximum displacement of the net truss was affected by the wind angle and wind load standard value; the single factor influence was significant.

Figure 18 shows the relationship between different wind angles and standard values of wind load on the displacement of the net truss. It is shows that under the two-factor combination of wind angle and wind load standard value, the structural deformation displacement of the net truss can be roughly divided into three intervals. In the wind load standard value range of 0–1.0 kN/m^2, the overall net truss deformation was less affected by the different wind angles. The deformation displacement was in the interval of 0–20 mm, and the growth rate of structural deformation displacement of the net truss increased significantly in the wind load range of 1.0–1.4 kN/m^2. In the wind load range of 1.0–1.4 kN/m^2, the growth rate of structural deformation and displacement increased significantly, the effect of wind load in the 0° and 180° wind angle direction on the structural response of the net truss increased gradually, and the overall structural displacement of the net truss was in the range of 20–32 mm. The net truss structure response was evident in the case of the standard wind load value $<$ 1.4 kN/m^2,

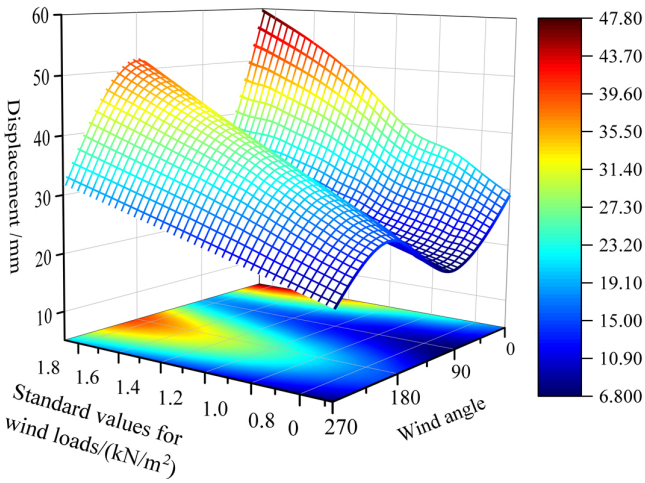

Fig. 18. Wind direction angle–wind load standard value displacement diagram

the growth rate of structural deformation and displacement increased, and the maximum structural displacement of the net truss occurred in the 0° and 180° directions. The maximum displacement of the net truss structure occurred at 0° and 180° direction angles, among which the 0° angle had the largest structural deformation. In summary, when the standard value of wind load was < 1.0 kN/m^2, the wind load impact on the overall structure of the net truss was small. When the standard value of wind load was > 1.0 kN/m^2, the deformation and displacement of the net truss structure in the 0° and 180° directions were the largest, which may affect the safety of the overall net truss structure.

6. Conclusions

In this paper, a static equivalent method for transferring the wind load on the roof surface and the nodal force of the internal rods of the large-span space net truss structure is proposed. The quasistatic tensile test of Q355B steel pipe material is conducted to provide the material parameters for the deformation of the structure. The equivalent static analysis of the main net truss of the roof is performed using the finite element software ANSYS, with Xintang Station in Guangzhou City, China, as an example, to explore the structural deformation of the whole structure under different standard values of the wind load working conditions. Structural deformation under different standard wind load conditions. The following conclusions are drawn:

1. By using the static equivalent method of wind load, the wind load on the face area is divided based on the node area ratio of the rods. This approach addresses the issue of local force inhomogeneity caused by the structural characteristics of the roof's appearance and enhances the accuracy of node displacement solutions in the wind load-sensitive areas of large-span spatial steel roof mesh trusses.

2. By observing the structural deformation under four wind load standard values (0.67 kN/m^2, 0.93 kN/m^2, 1.33 kN/m^2, and 1.87 kN/m^2), it is found that the wind load-sensitive zone of the steel roof trusses is consistent with the location of the wind load-sensitive zone. The greater the wind load, the more pronounced the structural deformation, which is not affected by the wind load acting on the roof surface. This further indicates that the sensitive zone of the steel roof net truss is related to the design of the roof profile and structural characteristics.
3. When the roof surface is subjected to various wind loads at different wind angles, the deformation of the large-span steel mesh truss structure varies significantly. Under four wind angles (0°, 90°, 180°, and 270°), the windward side corner contact area is the wind load-sensitive zone, experiencing the greatest overall structural deformation of the mesh truss. The deformation radiates from the largest contact surface of the wind load in a bow wave pattern in all directions. As the distance increases, the overall structural displacement and deformation of the mesh truss decrease. As the distance increases, the displacement and deformation of the overall truss net structure decrease.
4. The overall deformation analysis of the net truss under various wind angles and wind load combinations shows that as the wind load standard value increases, the deformation displacement of the net truss structure also increases. There is a linear correlation between the wind load standard value and the deformation displacement of the net truss structure. When the wind load standard value exceeds 1.0 kN/m^2, the deformation is greatest at 0° and 180° wind angles. This is related to the size of the vertical windward surface area and the spacing of steel columns. Therefore, in the design of large-span space structures, multiple wind-resistant defenses should be established on the windward side to prevent damage to local wind-resistant facilities from compromising the overall wind-resistant system.

References

[1] Y. Luo, X. Liu, H.P. Wan, and Y. Wang, "Field measurement of wind pressure on a large-scale spatial structure and comparison with wind tunnel test results", *Journal of Civil Structural Health Monitoring*, vol. 11, pp. 707–723, 2021, doi:10.1007/s13349-021-00477-w.

[2] E. Gavanski and H. Nishimura, "Wind loads on multi-span roof buildings", *Journal of Wind Engineering and Industrial Aerodynamics*, vol. 220, art. no. 104824, 2021, doi:10.1016/j.jweia.2021.104824.

[3] P. Woźniczka, "Fire Resistance Assessment of the Long-Span Steel Truss Girder", *Archives of Civil Engineering*, vol. 66, no. 2, pp. 63–75, 2020, doi:10.24425/ace.2020.131796.

[4] M. Kawaguchi, "Design problems of long span spatial structures", *Engineering Structures*, vol. 13, no. 12, pp. 144–163, 1991, doi:10.1016/0141-0296(91)90048-H.

[5] P. Bernandin, "Constructional steel design for structures with a dominant wind bora load", *Journal of Constructional Steel Research*, vol. 46, no. 1–3, pp. 321–322, 1998, doi:10.1016/S0143-974X(98)80040-0.

[6] Y.X. Li, S. Bai, Q.S. Yang, et al., "Experiment study on non-Gaussian distribution of fluctuating wind load on long-span enclosed", *Journal of Building Structures*, vol. 40, no. 7, pp. 62–69, 2019, doi:10.14006/j.jzjgxb.2018.0002.

[7] C. Maraveas and K.D. Tsavdaridis, "Assessment and retrofitting of an existing steel structure subjected to wind-induced failure analysis", *Journal of Building Engineering*, vol. 23, pp. 53–67, 2019, doi:10.1016/j.jobe.2019.01.005.

[8] G. Frontini, et al., "Advances in the application of the Principal Static Wind Loads: A large-span roof case", *Engineering Structures*, vol. 262, art. no. 114314, 2022, doi:10.1016/j.engstruct.2022.114314.

[9] L. Patruno, M. Ricci, S de Miranda, et al., "Equivalent Static Wind Loads: Recent developments and analysis of a suspended roof", *Engineering Structures*, vol. 148, pp. 1–10, 2017, doi:10.1016/j.engstruct.2017.05.071.

[10] N. Yang and F. Bai, "Damage Analysis and Evaluation of Light Steel Structures Exposed to Wind Hazards", *Applied Sciences*, vol. 7, no. 3, pp. 239, 2017, doi:10.3390/app7030239.

[11] Z.K. Wang, X.H. Wang, H. Zhao, et al, "Equivalent static wind loads on canopies of regular railway stations", *Engineering Structures*, vol. 276, art. no. 115336, 2023, doi:10.1016/j.engstruct.2022.115336.

[12] W.T. Shen, Y.W. Zeng, W.R. Zhang, et al., "Structural design and simulation analysis of fixed adjustable photovoltaic support", *Journal of Computational Methods in Sciences and Engineering*, vol. 23, no. 3, pp. 1409–1423, 2023, doi:10.3233/JCM-226647.

[13] T.T. Ma, L. Zhao, T.F. Ji, and T. Tang, "Case study of wind-induced performance and equivalent static wind loads of large-span open-able truss structures", *Thin-Walled Structures*, vol. 175, art. no. 109206, 2022, doi:10.1016/j.tws.2022.109206.

[14] X.Y. Li, Y.G. Wang, Q. Chu, et al., "Wind-induced response monitoring of large-span air-supported membrane structure coal-shed under the influence of typhoons", *Thin-Walled Structures*, vol. 181, art. no. 109951, 2022, doi:10.1016/j.tws.2022.109951.

[15] W. Xu, Q.X. Li, "Research on the wind load and wind effects of long-span structures of high-speed train station", *Industrial Construction*, vol. 48, no. 3, pp. 78–82+126, 2018, doi:10.13204/j.gyjz201803016.

[16] T. Wo, J. W. Zhang, J.Y. Chen, et al., "Partitioned Equivalent Static Wind Load Research for Zhanjiang New Airport Terminal Roof Structure", *Progress in Steel Building Structures*, vol. 24, no. 06, pp. 92–100, 2022, doi:10.13969/j.cnki.cn31-1893.2022.06.010.

[17] G. Yao, C.Y. Wu, and Y. Yang, "Scientometric Analysis for Mechanical Performance of Broken-Line Long-Span Steel Structure in Construction Considering Geometric Nonlinearity", *Symmetry*, vol. 13, no. 7, art. no. 1229, 2021, doi:10.3390/sym13071229.

[18] J. Wang, J.D. Zhao, T. Lan, et al., "Development Progress and Future Prospect of Large-span Spatial Structures", *Building Science*, vol. 29, no. 11, pp. 2–10, 2013, doi:10.13614/j.cnki.11-1962/tu.2013.11.002.

[19] H. Montazeri and B. Blocken, "New generalized expressions for forced convective heat transfer coefficients at building facades and roofs", *Building and Environment*, vol. 119, pp. 153–168, 2017, doi:10.1016/j.buildenv.2017.04.012.

[20] Y. Yang, J.Z. Huang, and X.Y. Li, "The effect of the bolt spacing on the performance of the steel-aluminum composite mullions of curtain wall", *Thin-Walled Structures*, vol. 117, pp. 239–246, 2017, doi:10.1016/j.tws.2017.04.020.

[21] L.G. Zhang and W.J. Lou, "equivalent static wind load for multiple targets of large-scale space truss structure", *Engineering Mechanic*s, vol. 30, no. 08, pp. 148–154, 2013, doi:10.6052/j.issn.1000-4750.2012.05.0313.

[22] A .Padewska-Jurczak, D. Cornik, R. Walentynski, et al., "Research on the dynamics of lightweight shell and spatial structures with the aid of computational fluid dynamics and a shaking table", *Archives of Civil Engineering*, vol. 69, no. 4, pp. 379–392, 2023, doi:10.24425/ace.2023.147665.

[23] G. Gruben, M. Langseth, E. Fagerholt, et al, "Low-velocity impact on high-strength steel sheets: An experimental and nu-merical study", *International Journal of Impact Engineering*, vol. 88, pp.171, 2016, doi:10.1016/j.ijimpeng.2015.10.001.

[24] Load Code for the Design of Building Structures, GB 50009–2012. Beijing: Chinese Architecture &Building Press, 2012.

[25] X. Jiang, Z. Yin, and H. Cui, "Wind Tunnel Tests and Numerical Simulations of Wind-Induced Snow Drift in an Open Stadium and Gymnasium", *Advances in Civil Engineering*, vol. 2020, art. no. 8840759, 2022, doi:10.1155/2020/8840759.

[26] R Fizzo, V. Sepe, and M.F Sabbà, "Investigation of the Pressure Coefficients Correlation Field for Low-Rise Building Roofs", *Applied Sciences*, vol. 12, no. 21, art.no. 10790, 2022, doi:10.3390/app122110790.

[27] A. Pratap and N. Rani, "Study of the wind-induced effects on various roof angles of a mono-slope canopy roof using wind tunnel testing and computational fluid dynamics", *Sādhanā*, vol. 48, art. no. 167, 2023, doi:10.1007/s12046-023-02199-9.

Received: 2024-03-01, Revised: 2024-06-11